JOM, Vol. 65, No. 12, 2013
DOI: 10.1007/s11837-013-0733-x

A Successful Synthesis of the $CoCrFeNiAl_{0.3}$ Single-Crystal, High-Entropy Alloy by Bridgman Solidification

S.G. MA,[1] S.F. ZHANG,[1] M.C. GAO,[2,3] P.K. LIAW,[4] and Y. ZHANG[1,5]

1.—High-Entropy Alloys Research Center, State Key Laboratory for Advanced Metals and Materials, University of Science and Technology Beijing, Beijing 100083, People's Republic of China. 2.—National Energy Technology Laboratory, Albany, OR 97321, USA. 3.—URS Corporation, Albany, OR 97321, USA. 4.—Department of Materials Science and Engineering, The University of Tennessee, Knoxville, TN 37996, USA. 5.—e-mail: drzhangy@ustb.edu.cn

For the first time, a face-centered-cubic, single-crystal $CoCrFeNiAl_{0.3}$ (designated as Al0.3), high-entropy alloy (HEA) was successfully synthesized by the Bridgman solidification (BS) method, at an extremely low withdrawal velocity through a constant temperature gradient, for which it underwent two BS steps. Specially, at the first BS step, the alloy sample underwent several morphological transitions accompanying the crystal growth from the melt. This microstructure evolves from as-cast dendrites, to equiaxed grains, and then to columnar crystals, and last to the single crystal. In particular, at the equiaxed-grain region, some visible annealing twins were observed, which indicates a low stacking fault energy of the Al0.3 alloy. Although a body-centered-cubic CoCrFeNiAl (Al1) HEA was also prepared under the same conditions, only a single columnar-crystal structure with instinctively preferential crystallographic orientations was obtained by the same procedure. A similar morphological transition from dendrites to equiaxed grains occurred at the equiaxed-grain region in Al1 alloy, but the annealing twins were not observed probably because a higher Al addition leads to a higher stacking fault energy for this alloy.

INTRODUCTION

For a long time, the traditional alloy-design strategy was based on one or two principal metal elements that dictated the primary phase, while minor alloying elements that promote the formation of the secondary phase(s) were added in order to tailor the microstructures and properties.[1,2] Well-known examples are Al-, Mg-, Fe-, Ni-, and Cu-based alloys,[3] which are developed for various household and industrial applications. However, a limit of this traditional design approach has been that the useful alloy families are limited to a handful of those well-known elements (e.g., Al, Mg, Fe, Ni, and Cu) in the periodic table, although continuing effort in minor additions of alloying elements for marginally enhanced properties are still considered state-of-the-art usage. Recently, a novel alloy-design concept, wherein all the alloying elements are equally or near-equally mixed in a system[4] demonstrates that the total number of useful alloys can be surprisingly large. Taking an example of picking ten elements from the periodic table, the total number of quinary alloys for which each element has a composition of 20 at.% would be $C_{10}^{5} = \frac{10!}{5! \times 5!} = 252$.

This multiprincipal elements alloy usually contains more than five elements and was named high-entropy alloys (HEAs) by Yeh et al.[5] on the basis of the high configurational entropy of mixing. However, only carefully chosen elements can form an extensive solid solution in the face-centered-cubic (FCC) and body-centered-cubic (BCC) structures rather than intermetallic compounds,[6–9] and unique properties may result.[10–18] In particular, these properties include high wear resistance,[13] excellent fatigue behavior, [14] the optical balance of high-saturation magnetization, electrical resistivity, malleability,[15] superior tensile high-temperature elongation,[16] and significant high-temperature compressive strength.[17] These impressive properties make HEAs promising engineering materials

(Published online August 22, 2013)

especially for high-temperature applications, such as the turbine blades in aircraft engines, which are made of expensive nickel-based superalloys.[1]

While progress has been made in HEAs, as mentioned above, they all have a polycrystalline microstructure regardless of whether they have a single-phase or multiple-phase microstructure. Although grain-boundary segregation is generally not expected in HEAs due to the small difference in the atomic size among major constituent elements, laboratory solidification usually follows a nonequilibrium cooling path, which may result in compositional inhomogeneity. This trend may be aggravated by the sluggish diffusion kinetics, which is a characteristic of HEAs. Therefore, there is urgent need in producing single-crystal HEAs for which the composition is homogeneous and property characterization will truly represent HEAs from a viewpoint of fundamental understanding. The present study was undertaken as the first step in synthesizing single crystals of HEAs using the Bridgman solidification. As a result, a single-crystal FCC HEA was prepared successfully for the first time, and this report details the synthesis process and microstructure evolution of the single-crystal HEA.

On the other hand, it is known that grain boundaries (GBs) as a plane defect widely exist in polycrystalline materials. They are shortcut paths for high diffusivity, and often they act as an easy nucleation site for cracks that lead to fracture. This intrinsic limitation associated with GB has invoked the development of single-crystal superalloys, such as the nickel-based single-crystal superalloys. These materials are widely used in aircraft and power-generation turbines, rocket engines, and other challenging environments, including nuclear-power and chemical-processing plants.[1] The nickel-aluminum system is one key binary material among the nickel-based superalloy family, which is mainly responsible for the existence of coherent γ–γ' microstructures.

EXPERIMENTAL PROCEDURES

Two alloy ingots of nominal compositions of $CoCrFeNiAl_x$ (x value in a molar ratio, and x = 0.3 and 1, denoted by Al0.3 and Al1, respectively) were synthesized by arc-melting pure elements with a purity higher than 99.95 wt.% under a high-purity argon atmosphere on a water-cooled Cu hearth. The alloys were remelted at least four times to obtain chemical homogeneity. Then, the synthesized alloys were crashed into pieces and placed in an alumina tube with an internal diameter of 3 mm and a wall thickness of ~1 mm. Next, the samples were inductively heated to the completely melting condition by adjusting the heating power, holding for 15 min. The Bridgman solidification (BS) was carried out with a withdrawal velocity (V) of 5 μm/s through a temperature gradient (G) of about 45 K/mm into the water-cooled Ga-In-Sn liquid alloys, for which a systematic diagram is shown in Fig. 1. In this experiment, two BS steps were conducted, which means that after the first BS step, the same sample was turned by 180° lengthwise, and the BS was repeated under the same conditions as the first BS process. Cylindrical samples were cut open along the longitudinal direction and then ground, polished, and etched. The microstructure evolution of the synthesized specimens was investigated by a metallographic microscope.

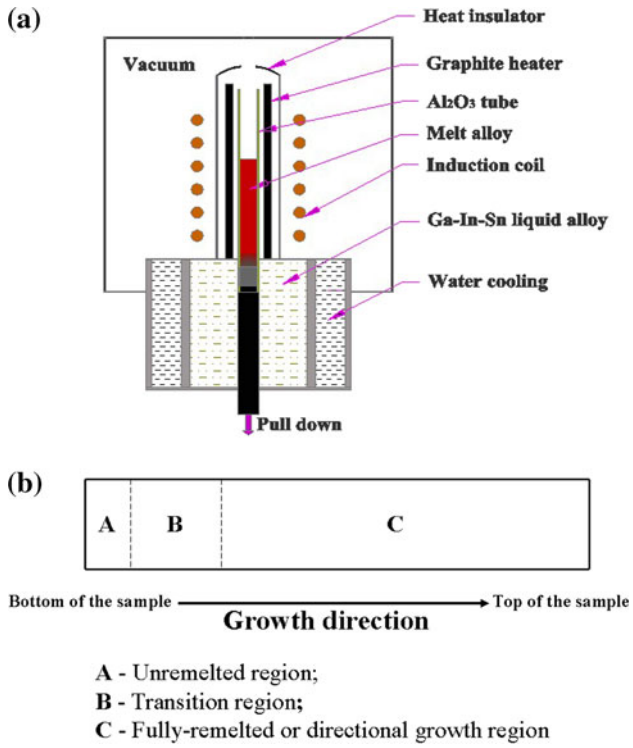

Fig. 1. A systematic diagram of the Bridgman-solidification technique: (a) the experimental process and (b) the sample location.

RESULTS AND DISCUSSION

Figure 2 demonstrates the optical micrographs of microstructure evolution for Al0.3 HEA by BS under the withdrawal velocity of 5 μm/s. These microstructural morphologies are derived from the same alloy sample but different sites of the sample, as shown in Fig. 2a–d. In each figure, the single long arrow stands for the growth direction of the microstructure. Figure 2a shows a typical network-like dendrites and interdendrites morphology, for which it stems from the un-remelted region A of the alloy sample (or the bottom of the alloy sample at the closest region to the water-cooled Ga-In-Sn liquid alloy surface) and thus remains the as-cast microstructure.

Along the growth direction of the microstructure or away from the bottom of the alloy sample (the transition region B), an obvious morphological transition from dendrites to equiaxed grains can be

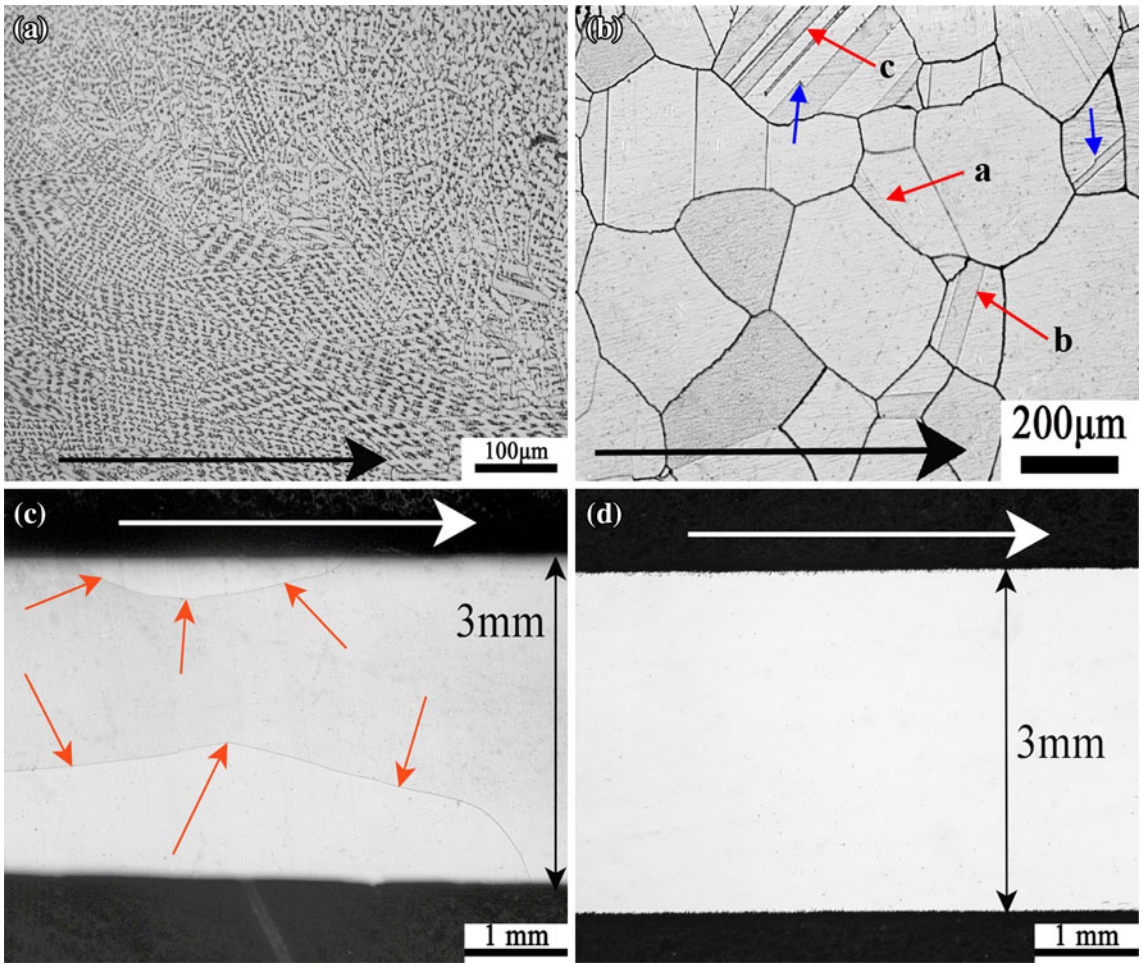

Fig. 2. The optical microphotos of microstructure evolution for the $CoCrFeNiAl_{0.3}$ high-entropy alloy by Bridgman solidification: (a) as-cast dendrites; (b) equiaxed grains embedded with twinning crystals; (c) columnar crystals; and (d) single crystal.

found in Fig. 2b, and a similar phenomenon was reported in our previous work.[19] This feature is probably ascribed to the following reasons: (I) The thermal-diffusion effect acts as the driving force for the annihilation or remelting of the interdenrites with a relatively lower melting point than dendrites and promotes the growth and coarsening of the primary dendrites, on the basis of the heat-affected region for the alloy sample location; (II) a larger value of the G/V (the temperature gradient to the growth velocity ratio) set the conditions for the planar solidification front retaining and, thus, enables the formation of an equiaxed-grain structure as referred to in the literature;[19] and (III) the residual thermal stress introduced by the as-cast process may be also responsible for the microstructure transition. These equiaxed grains have a wide size range of about 50 μm–300 μm, in which some visible annealing-twin-like crystals with an average width of several tens micrometer were captured, as shown in Fig. 2b. In particular, Fig. 2b reveals three typical annealing-twin morphologies,[20] which are characterized as annealing twins close to the grain boundary (a), complete annealing twins across the grain matrix (b), and incomplete annealing twins where one end terminates in the grain (c), as marked by the red arrows in Fig. 2b.

It is known that annealing twins were often observed in FCC metals or alloys, such as brass, austenitic stainless steels, or even nickel-based superalloys,[20,21] under the cold deformation and subsequent recrystallization-annealing process. Two representative models for the formation mechanism of annealing twins have been previously proposed.[21–23] One is the growth accident model,[22] which means that annealing twins are generally due to the incorrect arrangement of the atomic layers along the (111) crystallographic plane during the growth of the crystal by the migration of the grain boundary. The other is a model[23] that involves nucleation twins by staking faults or fault packets at the intersection of three grain boundaries. In other words, the lower the stacking fault energy, the more the number of stacking faults, and thus, the formation of annealing twins is easier for a material. Our findings indicate that this HEA may have low stacking fault energy. In addition, the former model promotes the formation of coherent annealing-twin boundaries, while the latter

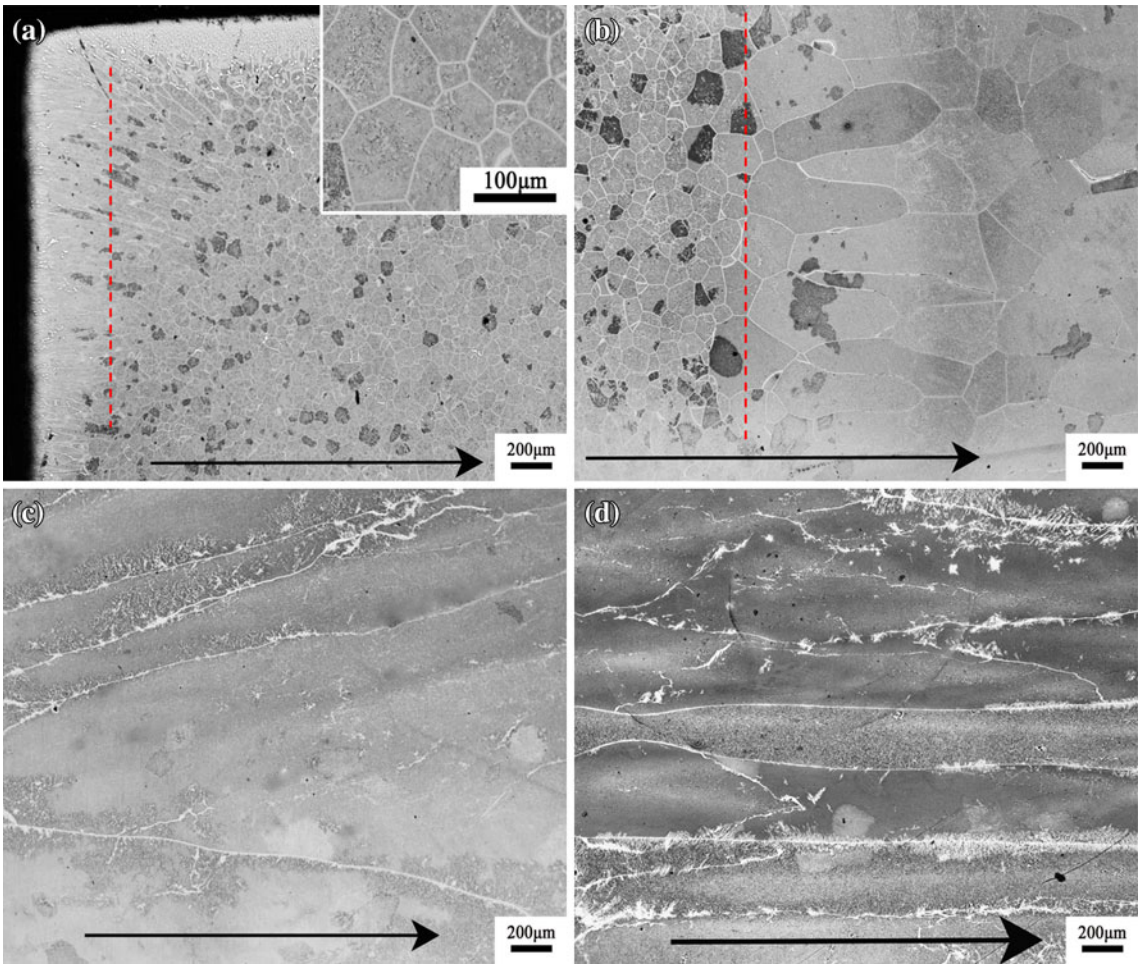

Fig. 3. The optical microphotos of microstructure evolution for the CoCrFeNiAl high-entropy alloy by Bridgman solidification: (a) a mixture of as-cast dendrites and equiaxed grains; (b) an obvious transition from equiaxed grains to columnar crystals; (c) columnar crystals grown inclined around 30° to the growth direction; and (d) columnar crystals grown parallel to the growth direction.

favors the incoherent annealing-twin boundary. In this HEA alloy, it can be noted that some incoherent twin boundaries are present in this alloy as the step at the twin-boundary line denoted by the blue arrows in Fig. 2b. The presence of both common coherent and incoherent twin boundaries indicates that a mixed model is required to explain the formation of these annealing twins. Additionally, these annealing twins can effectively decrease the Gibbs free energy of the system and improve its thermodynamic stability, based on a much lower interfacial free energy for the twin boundary than the grain boundary. It has been previously reported that the occurrence of twinning, probably due to the existence of thermal supercooling near to the surface of the crystal, could result in the presentation of an interface more favourably oriented for growth in the local heat flow direction near to the edges of the specimen.[24] Hence, the formation of twining that is often accidental may be helpful to the evolution of the anticipated columnar grains or even a single crystal.

Subsequently, the remaining alloy was located at a fully remelted region C. As the solid/liquid interface advanced during solidification, another morphology transition from the equiaxed-grain structure to columnar-grain structure occurred in this alloy. The bulky columnar-grain boundary with a millimeter scale can be clearly captured, as denoted by the red arrows in Fig. 2c. This feature is due to the significant preferential growth of some grains with favorable crystallographic orientation, mostly at inclined angles to the growth direction, on the basis of an extremely low-grain-growth velocity of about 5 μm/s (here the grain-growth velocity approximately equals that of the withdrawal velocity).

Finally, in the upmost part of the sample, only one grain with the optical crystallographic orientation was produced, with the columnar-grain boundary completely disappeared, as shown in Fig. 2d. In other words, a single-crystal growth was achieved via planar interface through a controlled directional solidification process. These controlled conditions include a moderate temperature gradient, a slow growth rate, a high vacuum atmosphere, and a steady diffusion of heat along the length of the sample that was achieved in the experiment, all of

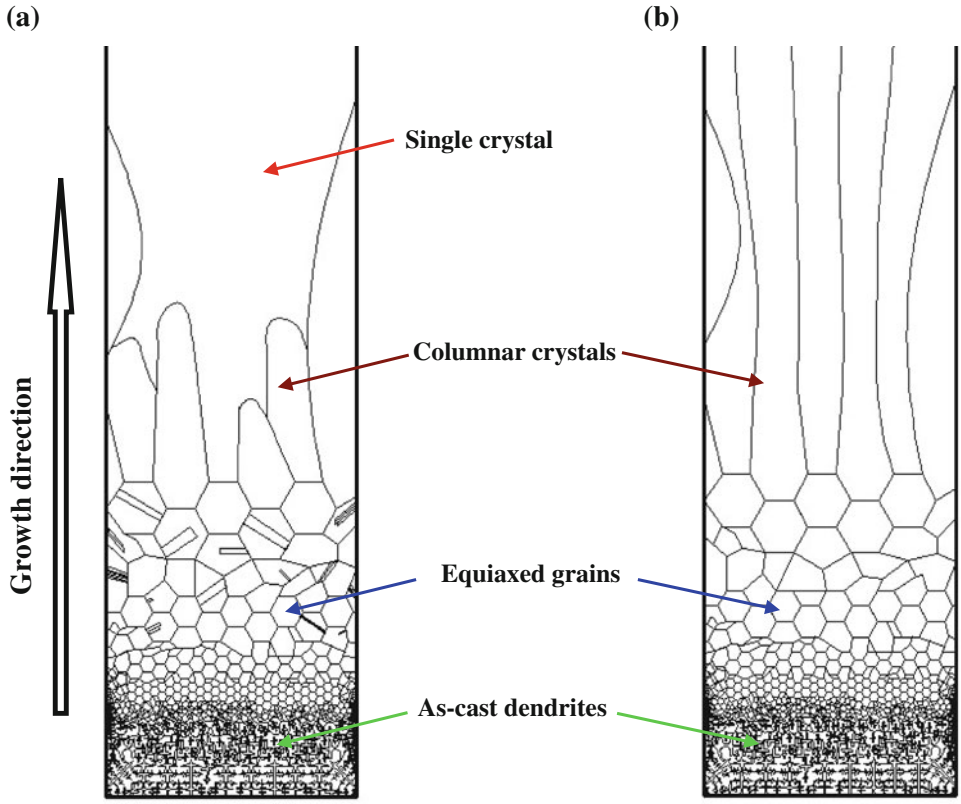

Fig. 4. A systematic diagram of microstructure evolution for the $CoCrFeNiAl_{0.3}$, (a), and CoCrFeNiAl, (b), high-entropy alloys by Bridgman solidification.

which may be conducive to the competitive growth of grains with preferred orientations. Next, as referred to in the experimental procedure, after the first BS step, the solidified alloy sample was subsequently inverted, and thus the upmost single-crystal part was partly located in the unmelted region A of Fig. 1b, serving as a seed,[24] and then another BS step was conducted upon the same sample under the initial conditions; i.e., the remaining solid alloy was again heated to melt and the whole melt was expected to solidify into a single crystal as the solid–liquid interface advanced away from the seed. A similar solidification process was reported in the preparation of one lamellar grain of the Ti-46Al-5Nb alloy.[25] As a consequence, after the second growth, a complete single-crystal Al0.3 HEA with a diameter of 3 mm and a length of about 50 mm was successfully obtained.

For comparison, the same BS process was carried out upon the BCC Al1 HEA, and the corresponding optical micrographs of microstructure evolution were presented in Fig. 3. Figure 3a–c exhibit the microstructure-growth process at the first BS step, while Fig. 3d displays the microstructural morphology after the second growth. Similarly, in each figure, the single long arrow stands for the growth direction of the microstructure. A similar changing trend (the dendrites to the equiaxed-grain transition) for the microstructure evolution on this alloy, as found in the FCC Al0.3 alloy, was definitely observed in Fig. 3a–c. Figure 3a shows a mixed microstructure of as-cast dendrites and equiaxed grains, where the dendrites of a small volume fraction are closely located at the bottom of the sample (i.e., on the left side of the micrograph), and the equiaxed grains of a large volume fraction with an average grain size of 50 μm are homogeneously distributed at the alloy surface. Nonetheless, annealing twins were not observed in this alloy as confirmed by the upper-right inset of Fig. 3a. This feature differs from the Al0.3 alloy as the Al element generally has high stacking fault energies of around 160 mJ/m–200 mJ/m^2, [26] in which twinning crystals are difficult to observe. It is tempting to suggest that higher Al concentration probably causes higher stacking fault energy and that, consequently, annealing twins were not observed in the Al1 alloy.

With the BS continued, the equiaxed grains gradually coarsened and elongated, which ultimately led to the morphology transition from equiaxed grains to columnar grains where the transition boundary (the dashed line) can be clearly captured, as shown in Fig. 3b. As the solid/liquid interface continues to advance during solidification, Fig. 3c exhibits more obvious columnar-grain crystals with an average size of several hundreds of micrometers. The columnar boundary is inclined at ~30° to the microstructural-growth or heat-flow direction. After

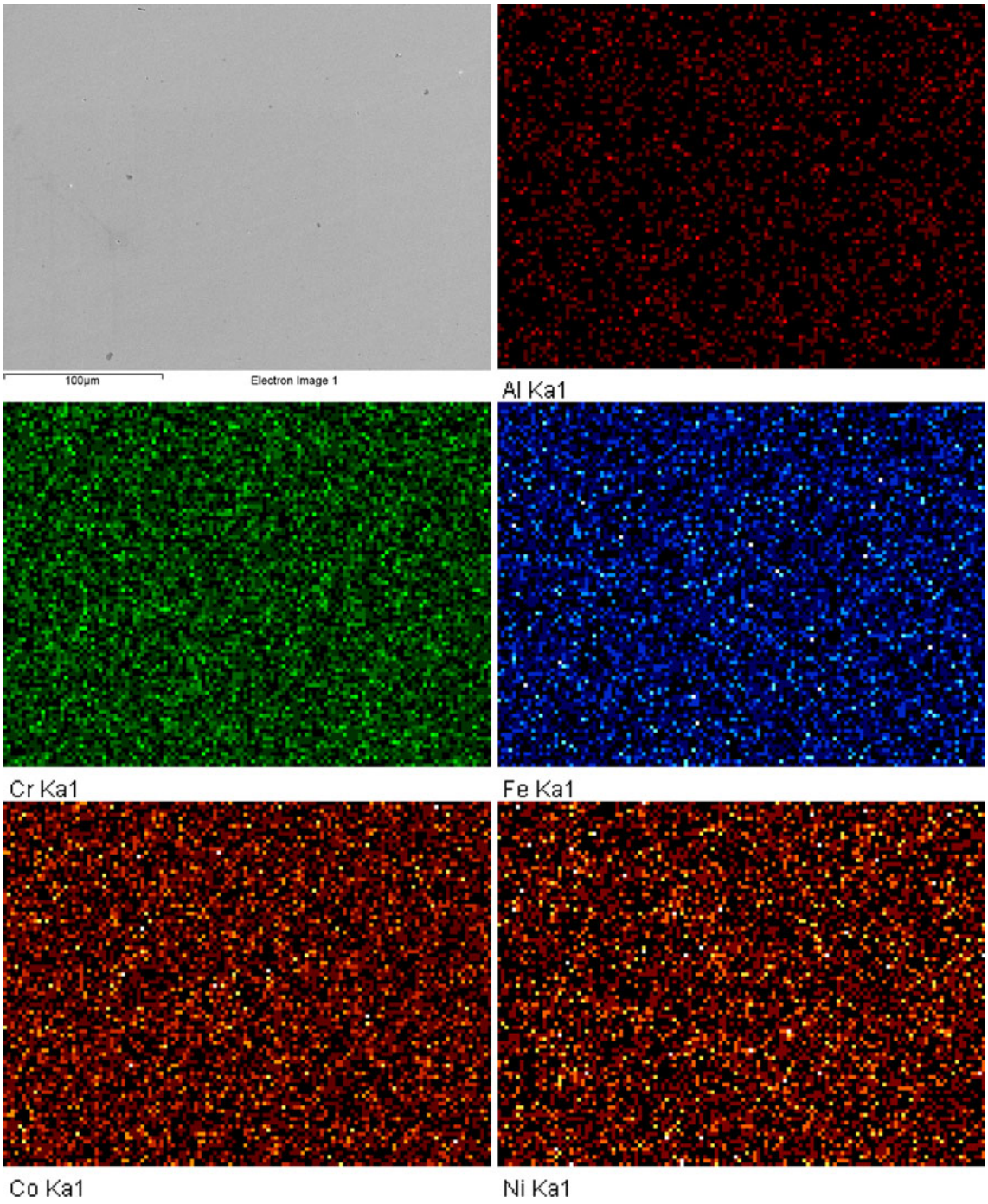

Fig. 5. Energy dispersive spectroscopy of the single-crystal part of the $CoCrFeNiAl_{0.3}$ alloy. The relative intensity of each element map gives a qualitative sense for the distributed characteristics of those constituents.

the second BS step, the columnar boundaries are aligned parallel to the growth direction as shown in Fig. 3d. Clearly the attempt to produce a single-crystal Al1 alloy in the BCC structure by the two BS steps failed.

To compare the solidification behavior of these two alloys, a systematic diagram of the microstructure evolution for the Al0.3 (Fig. 4a) and Al1 (Fig. 4b) HEAs by BS technique was presented in Fig. 4. As addressed by the analyses above, the FCC Al0.3 alloy underwent a microstructural transition from dendrites to equiaxed grains, and then to columnar grains, and last to a single-crystal structure. But for the BCC phase, the attempt is not successful. The BCC Al1 alloy went through almost the same mcirostructural transition process, but the final-stage solidification structure consists of columnar crystals not of a single crystal under the

same conditions. These features can be clearly demonstrated in Fig. 4. As a result, by two BS steps, we finally obtained the single-crystal FCC Al0.3 alloy and columnar-crystal BCC Al1 alloy.

This present study indicates that a single crystal of HEAs in the FCC structure is easier to synthesize than a BCC HEA. Comparing the chemical compositions of the two alloys suggests that the Al element in the alloys is mainly responsible for the different solidification behavior. A higher Al content introduces more negative enthalpy of mixing,[27] larger atomic-size difference,[27] and larger density gradient. However, the underlying reason has yet to be further investigated and clarified. In addition, as stated above, a low Al content can induce a low stacking fault energy and, thus, the generation of twinning crystals during BS process. In other words, the Al addition can effectively tailor the stacking fault energy or potential twinning-crystal density (under appropriate conditions) of the alloy system, for which it has been successfully applied to improve the tensile ductility of metallic alloys (e.g., Fe-6.5 wt.% Si alloy[28] or bulk metallic glass composites[29]). Compared with the nickel-based superalloys, whose directionally solidified microstructures are distinctly dendrites-mircrosegregated,[1] the present alloys display a planar-interface growth mode of the microstructure, i.e., the elimination of the as-cast dendrites segregation, as shown in Figs. 2–4. Moreover, Fig. 5 displays the energy dispersive spectroscopy of the single-crystal part of the Al0.3 alloy. As presented from each element map, this alloy exhibits a relatively uniform elemental distribution that indicates a segregate-free characteristic. These features may point to a potential direction for the high-temperature application of HEAs.

CONCLUSIONS

Using two BS steps, we first successfully prepared the FCC-structured, single-crystal Al0.3 HEA, and the BCC-structured, columnar-crystal Al1 HEA, with instinctively preferential crystallographic orientations, under an extremely slow growth velocity. The single-crystal sample is of the order of 3 mm in diameter and about 50 mm in length. In addition, at the first BS step, along with the growth direction of the microstructure, several obvious morphological transitions were definitely observed from the bottom to the top of the sample in these two alloys. The microstructure of the Al0.3 alloy started with the dendrites, and then underwent equiaxed grains and columnar crystals, and lastly ended with the single crystal, while for the Al1 alloy, only the last transition was not obtained. Interestingly, in the equiaxed-grain region of the Al0.3 alloy, some annealing-twin-like crystals with a twin-boundary spacing of about several tens of micrometers were observed. The ready-to-wear growth models for annealing twins indicate that the Al0.3 alloy may have a low stacking fault energy. However, they were not observed in the Al1 alloy that was probably ascribed to a higher Al content, leading to a higher stacking fault energy.

ACKNOWLEDGEMENTS

The authors are grateful for the Program for National Natural Science Foundation of China (NNSFC) (Contract No: 50971019). MCG acknowledges support of the Innovative Processing and Technologies Program of the National Energy Technology Laboratory's (NETL) Strategic Center for Coal under the RES Contract DE-FE-0004000. PKL very much appreciates the financial support from the U.S. National Science Foundation (DMR-0909037, CMMI-0900271, and CMMI-1100080), the Department of Energy (DOE), Office of Nuclear Energy's Nuclear Energy University Programs (NEUP) 00119262, and the DOE, Office of Fossil Energy, National Energy Technology Laboratory (DE-FE-0008855) with C. Huber, C. V. Cooper, D. Finotello, A. Ardell, E. Taleff, V. Cedro, R. O. Jensen, L. Tan, and S. Lesica as contract monitors.

REFERENCES

1. T.M. Pollock and S. Tin, *J. Propuls. Power* 22, 361 (2006).
2. J.W. Qiao, A.C. Sun, E.W. Huang, Y. Zhang, P.K. Liaw, and C.P. Chuang, *Acta Mater.* 59, 4126 (2011).
3. K. Lu, *Science* 328, 319 (2010).
4. B. Cantor, I.T.H. Chang, P.K. Night, and A.J. Vincent, *Mater. Sci. Eng. A* 375, 213 (2004).
5. J.W. Yeh, S.K. Chen, S.J. Lin, J.Y. Gan, T.S. Chen, T.T. Shun, C.H. Tsau, and S.Y. Chang, *Adv. Eng. Mater.* 6, 299 (2004).
6. Y. Zhang, Y.J. Zhou, J.P. Lin, G.L. Chen, and P.K. Liaw, *Adv. Eng. Mater.* 10, 534 (2008).
7. X. Yang and Y. Zhang, *Mater. Chem. Phys.* 132, 233 (2012).
8. Y. Zhang, X. Yang, and P.K. Liaw, *J. Miner. Met. Mater. Soc.* 64, 830 (2012).
9. C. Zhang, F. Zhang, S. Chen, and W. Cao, *JOM* 64, 839 (2012).
10. Y.J. Zhou, Y. Zhang, Y.L. Wang, and G.L. Chen, *Appl. Phys. Lett.* 90, 181904 (2007).
11. X.F. Wang, Y. Zhang, Y. Qiao, and G.L. Chen, *Intermetallics* 15, 357 (2007).
12. S.G. Ma and Y. Zhang, *Mater. Sci. Eng. A* 532, 480 (2012).
13. M.H. Chuang, M.H. Tsai, W.R. Wang, S.J. Lin, and J.W. Yeh, *Acta Mater.* 59, 6308 (2011).
14. M.A. Hemphill, T. Yuan, G.Y. Wang, J.W. Yeh, C.W. Tsai, A. Chuang, and P.K. Liaw, *Acta Mater.* 60, 5723 (2012).
15. Y. Zhang, T.T. Zuo, Y.Q. Cheng, and P.K. Liaw, *Sci. Rep.* 3, 1455 (2013).
16. A.V. Kuznetsov, D.G. Shaysultanov, N.D. Stepanov, G.A. Salishchev, and O.N. Senkov, *Mater. Sci. Eng. A* 533, 107 (2012).
17. O.N. Senkov, G.B. Wilks, J.M. Scott, and D.B. Miracle, *Intermetallics* 19, 698 (2011).
18. Y. Zhang, T.T. Zuo, Z. Tang, M.C. Gao, K.A. Dahmen, P.K. Liaw, and Z.P. Lu, *Prog. Mater. Sci.* (in press).
19. Y. Zhang, S.G. Ma, and J.W. Qiao, *Metall. Mater. Trans. A* 43A, 2625 (2012).
20. S. Mahajan, C.S. Pande, M.A. Imam, and B.B. Rath, *Acta Mater.* 45, 2633 (1997).
21. C.S. Pande, M.A. Imam, and B.B. Rath, *Mater. Trans.* 21A, 2891 (1990).
22. H. Gleiter, *Acta Metall.* 17, 1421 (1969).
23. S. Dash and N. Brown, *Acta Metall.* 11, 1067 (1963).
24. D.T.J. Hurle, *Mechanisms of Growth of Metal Single Crystals from the Melt* (Oxford: Pergamon Press Ltd, 1962).

25. X.F. Ding, J.P. Lin, L.Q. Zhang, Y.Q. Su, and G.L. Chen, *Acta Mater.* 60, 498 (2012).
26. L.E. Murr, *Interfacial Phenomena in Metals and Alloys* (Reading: Addison-Wesley Publishig Co, 1975).
27. A. Takeuchi and A. Inoue, *Metall. Mater. Trans.* 46, 2817 (2005).
28. J.X. Xie, H.D. Fu, Z.H. Zhang, and Y.B. Jiang, *Intermetallics* 23, 20 (2012).
29. Y. Wu, D.Q. Zhou, W.L. Song, H. Wang, Z.Y. Zhang, D. Ma, X.L. Wang, and Z.P. Lu, *Phys. Rev. Lett.* 109, 245506 (2012).